Different physicochemical behaviors of nitrate and ammonium during transport: a case study on Mt. Hua, China

Can Wu[1], Cong Cao[2,a], Jianjun Li[2], Shaojun Lv[1], Jin Li[2,b], Xiaodi Liu[1], Si Zhang[1], Shijie Liu[1], Fan Zhang[1], Jingjing Meng[4], Gehui Wang[1,3]*

[1] Key Lab of Geographic Information Science of the Ministry of Education, School of Geographic Sciences, East China Normal University, Shanghai 200062, China
[2] State Key Laboratory of Loess and Quaternary Geology, Institute of Earth Environment, Chinese Academy of Sciences, Xi'an 710061, China
[3] Institute of Eco-Chongming, Chenjia Zhen, Chongming, Shanghai 202162, China
[4] School of Environment and Planning, Liaocheng University, Liaocheng 252000, China

[a] Now at The State University of New York at Stony Brook.
[b] Now at Institute for Environmental and Climate Research, Jinan University.

*Corresponding author. Gehui Wang (ghwang@geo.ecnu.edu.cn)

Abstract: To understand the chemical evolution of aerosols in the transport process, the chemistry of $PM_{2.5}$ and nitrogen isotope compositions on the mountainside of Mt. Hua (~1120 m a.s.l.) in inland China during the 2016 summertime were investigated and compared with parallel observations collected at surface sampling site (~400 m a.s.l.). $PM_{2.5}$ exhibited a high level at the surface (aver. 76.0±44.1 μg/m^3) and could be transported aloft by anabatic valley winds, leading to the gradual accumulation of daytime $PM_{2.5}$ with a noon peak at the mountainside sampling site. As the predominant ion species, sulfate exhibited nearly identical mass concentrations in both sites, but its $PM_{2.5}$ mass fraction was moderately enhanced by ~4% at the higher elevation. The ammonium variations were similar to the sulfate variations, the chemical forms of both of which mainly existed as ammonium bisulfate (NH_4HSO_4) and ammonium sulfate ($(NH_4)_2SO_4$) at the lower and higher elevations, respectively. Unlike sulfate and ammonium, nitrate mainly existed as ammonium nitrate (NH_4NO_3) in fine particles and exhibited decreasing mass concentration and proportion trends with increasing elevation. This finding was ascribed to NH_4NO_3 volatilization, in which gaseous HNO_3 from semi-volatile NH_4NO_3 subsequently reacted with dust particles to form nonvolatile salts, resulting in significant nitrate shifts from fine particles into coarse particles. Such scavenging of fine-particle nitrate led to an enrichment in the daytime ^{15}N of nitrate at the mountainside site compared with to the lower-elevation site. In contrast to nitrate, at the higher elevation, the ^{15}N in ammonium depleted during the daytime. Considering the lack of any significant change in ammonia sources during the vertical transport process, this ^{15}N depletion in ammonium was mainly the result of

unidirectional reactions, indicating that additional ammonia would partition into particulate phases and further neutralize HSO_4^- to form SO_4^{2-}. This process would reduce the aerosol acidity, with a higher pH (3.4±2.2) at mountainside site and lower ones (2.9±2.0) at mountain foot site. Our work provides more insight into physicochemical behaviors of semi-volatile nitrate and ammonium, which will facilitate the improvement in model for a better simulation of aerosol composition and properties.

Keywords: Ammonium; Nitrate; Stable nitrogen isotope; Haze; Volatilization

1 Introduction

Atmospheric particulate matter measuring equal to or less than 2.5 μm in aerodynamic diameter ($PM_{2.5}$) is a worldwide air pollution burden that can deteriorate the urban air quality and induce adverse human health effects that contribute to lowering life expectancies (Shiraiwa et al., 2017; Lelieveld et al., 2015; Fuzzi et al., 2015; Wang et al., 2016). Recent studies have disclosed that the mechanisms underlying these effects are profoundly dependent on particle properties, e.g., the size, concentration, mixing state and chemical compositions of particles (Li et al., 2016; Liu et al., 2021; Guo et al., 2014). Thus, since 2013, China has issued strict emission directives to mitigate haze pollution. Consequently, the annual $PM_{2.5}$ concentration in China fell by approximately one-third from 2013–2017 (Zheng et al., 2018). Notwithstanding, the $PM_{2.5}$ levels in most cities in China still exceed the least-stringent target of the World Health Organization (WHO 2021; 35 $\mu g/m^3$), especially in rural areas and small cities (Lv et al., 2022; Li et al., 2023).

Near-surface PM can also be transported to the upper air, and this process critically impacts radiative forcing, cloud precipitation and the regional climate by scattering/absorbing solar radiation and by influencing aerosol-could interactions (Van Donkelaar et al., 2016; Andreae and Ramanathan, 2013; Fan et al., 2018). Past assessments of these effects have been characterized by large uncertainties (Carslaw et al., 2013); for example, Bond et al. (2013) found that black carbon climate forcing varied from +0.17 W/m^2 to +2.1 W/m^2 with a 90% uncertainty. Such massive uncertainties are mainly due to our limited knowledge regarding the spatiotemporal

distribution, abundance and compositions of airborne PM (Seinfeld and Johnh, 2016; Raes et al., 2000). In addition, aerosols may undergo aging during the vertical transport process, causing increasingly complex compositions and changes in aerosol properties. Despite these factors, to date, vertical observations remain comparatively scarce compared to surface measurements. Therefore, to obtain an improved understanding of the fundamental chemical and dynamical processes governing haze development, more field observations of upper-layer aerosols are necessary, as these measurements could provide updated kinetic and mechanistic parameters that could serve to improve model simulations.

Currently, various monitoring approaches have been developed and applied to measure vertical aerosols, e.g., satellite remote sensing and in situ lidar methods; these approaches can be used to obtain the pollution concentration profiles (Van Donkelaar et al., 2016; Reid et al., 2017). To accurately measure chemical compositions, aircraft and unmanned aerial vehicles (UAVs) equipped with a variety of instruments can be utilized in short-term sampling campaigns (Lambey and Prasad, 2021; Zhang et al., 2017), but these tools are unsuitable for long-term continued observations due to their high operational costs. In cases of near-surface vertical urban atmosphere observations, techniques involving tethered balloons, meteorological towers and skyscrapers are usually adopted (Zhou et al., 2020; Xu et al., 2018; Fan et al., 2021). However, the vertical application range of these methods are limited to only ~500 m, thus hardly meeting the requirements of research conducted above the boundary layer. Therefore, high-elevation mountain sites have long been regarded as suitable places for long-term

research on the upper-layer aerosol (including its compositions, chemical-physical properties and formation processes, etc.) (Dzepina et al., 2015; Zhou et al., 2021; Wang et al., 2013), which are conducive to better understanding of the haze episodes in the lower troposphere. Although the fixed observation position is the key drawback of this monitoring approach, it has still been widely selected for use in various vertical observation campaigns, e.g., in past studies conducted in Salt Lake Valley (Baasandorj et al., 2017), in Terni Valley (Ferrero et al., 2012) and on Mt. Tai (Meng et al., 2018; Wang et al., 2011).

Mt. Hua adjoins the Guanzhong Basin of inland China, where haze pollution has been a persistent environmental problem (Wu et al., 2020b; Wu et al., 2021; Wang et al., 2016). In our previous studies conducted at the mountaintop of Mt. Hua, we found that air quality was significantly affected by surface pollution, and distinctive differences were found in the aerosol compositions and size distributions at the mountaintop compared to those measured at lower elevations ground level (Wang et al., 2013; Li et al., 2013). With the implementation of strict emission controls, the atmospheric environment in this region has changed dramatically from the SO_2/sulfate-dominated previous environment to the current NO*x*/nitrate-dominated environment (Baasandorj et al., 2017; Wu et al., 2020c). However, the fundamental chemical and dynamical processes driving this $PM_{2.5}$-loading explosion are unclear under the current atmospheric state with increasing O_3 and NH_3 levels. To better rationalize these processes, in this work, 4-hr integrated aerosol samples were synchronously collected on the mountainside and at the lower-elevation land surface, and the chemical

components and stable nitrogen isotope compositions of nitrate and ammonium were analyzed in the collected $PM_{2.5}$ samples. We compared the chemical compositions and diurnal cycles between the two sampling sites and then discussed the changes in the chemical forms of secondary inorganic ions during their vertical transport from lower to higher elevations. Our study revealed that nitrate and ammonium exhibited distinct physicochemical behaviors during the aerosol-aging process.

2 Experiment

2.1 Sample collection

In this campaign, the $PM_{2.5}$ samples were synchronously collected at two locations in the Mt. Hua area during the period from 27 August to 17 September 2016. One sampling site was located on a building belonging to the Huashan Meteorological Bureau (34°32′N, 110°5′E, 400 m a.s.l.) at the foot of Mt. Hua. Surrounded by several traffic arteries and dense residential and commercial buildings, as shown in Figure 1b, this site is an ideal urban station for studying the impacts of anthropogenic activities on local air quality and is referred to hereafter as the "MF" site. The mountainous sampling site (34°29′N, 110°3′E, 1120 m a.s.l.) was located approximately 8 km from the city site horizontally (Figure 1c) at an elevation of 720 m above the average Huashan town level of ~400 m (a.s.l.). This site was situated on a mountainside that experiences little anthropogenic activity due to its steep terrain and is abbreviated hereafter as the "MS" site. Furthermore, this location adjoins one of the larger valleys of Mt. Hua; therefore, the measurements taken at this location were strongly affected by the lower-elevation air pollutants transported upwards by the valley winds. At both measurement sites, the

$PM_{2.5}$ aerosol samples with a 4-hr interval in were collected onto prebaked (at 450°C for 6 hrs) quartz filters using high-volume (1.13-m^3/min) air samplers (Tisch Environmental, Inc., USA). All air samplers were installed on the roofs of buildings, approximately 15 m above the local ground surface. Furthermore, size-resolved aerosol sampling was synchronously conducted at two sites during summertime (10-22 August, 2020); and these samples with nine size bins (cutoff points were 0.43, 0.65, 1.1, 2.1, 3.3, 4.7, 5.8 and 9.0 μm, respectively) were collected using an Anderson sampler at an airflow rate of 28.3 L/min for ~72 h. After sampling, the filter samples were stored in a freezer (at -18°C) prior to analysis.

The hourly $PM_{2.5}$, NO*x* and O_3 mass concentrations were detected at the mountainside sampling site using an E-BAM, a chemiluminescence analyzer (Thermo, Model 42i, USA) and a UV photometric analyzer (Thermo, Model 49i, USA), respectively. At the MF site, only $PM_{2.5}$ was monitored, using another E-BAM, while the data of the other species were downloaded from the Weinan Ecological Environment Bureau (http://sthjj.weinan.gov.cn/). Meteorological data characterizing both sampling sites throughout the whole campaign were obtained from the Shaanxi Meteorological Bureau website (http://sn.cma.gov.cn/).

2.2 Chemical analysis

Four punches (1.5-cm diameter) of each aerosol sample were extracted into 10-mL Milli-Q pure water (18.2 MΩ) under sonication for 30 min. Subsequently, the extracts were filtered with 0.45-μm syringe filters and detected for water-soluble ions (Na^+, NH_4^+, K^+, Mg^{2+}, Ca^{2+}, SO_4^{2-}, NO_2^-, NO_3^- and Cl^-) by using ion chromatography; the

detection limit for these nine ions was < 0.01 μg/mL. A DRI-model 2001 thermal–optical carbon analyzer was used herein following the IMPROVE-A protocol to analyze the organic carbon (OC) and elemental carbon (EC) in each $PM_{2.5}$ filter sample (in 0.526 cm^2 punches). For more details regarding the utilized methods, readers can refer to our previous studies (Wu et al., 2020b).

To quantify the stable nitrogen isotope compositions of nitrate ($\delta^{15}N\text{-}NO_3^-$) and ammonium ($\delta^{15}N\text{-}NH_4^+$) in $PM_{2.5}$ samples, the filter samples were pretreated as described for the water-soluble ion analysis. The ammonium in the extracts (approximately half of the resulting solution) was oxidized by hypobromite (BrO^-) to nitrite (NO_2^-), which was subsequently reduced by hydroxylamine (NH_2OH) in a strongly acidic environment. The above product (N_2O) was then analyzed by a commercially available purge and cryogenic trap system coupled to an isotope ratio mass spectrometer (PT-IRMS). A bacterial method (*Pseudomonas aureofaciens*, a denitrifying bacterium without N_2O reductase activity) was used herein to convert the sample NO_3^- into N_2O, which was ultimately quantified through PT-IRMS. As revealed in previous studies (Fang et al., 2011), the presence of NO_2^- in aerosols may interfere with the denitrifier method when measuring $\delta^{15}N$. Nonetheless, NO_2^- generally composed tiny portions in most of our samples and, on average, contributed <1.0% to NO_3^-+NO_2^-. Thus, we believed that the proportion of NO_2^- in the sample was too small to affect the resulting $\delta^{15}N$ measurements based on the discussions reported by Wankel et al. (2010). More details regarding the analytical artifact and quality control protocols can be found elsewhere (Wu et al., 2021; Liu et al., 2014).

2.3 Concentration-weighted trajectory (CWT) analysis

CWT is a powerful tool used herein to reveal the potential spatial sources responsible for the high $PM_{2.5}$ loadings measured on Mt. Hua; this method has been used previously in similar studies (Wu et al., 2020c; Wu et al., 2020a). In this study, the CWT analysis was conducted using the Igor-based tool coupled with hourly $PM_{2.5}$ concentrations and 12-hr air mass backward trajectories that were simulated by using the Hybrid-Single Particle Lagrangian Integrated Trajectory (HYSPLIT) model (Petit et al., 2017).

2.4 Theoretical calculations of the partial pressures of NH_3 and HNO_3 and the dissociation constant of NH_4NO_3

To obtain the product of the partial pressures of NH_3 and HNO_3, the NH_4NO_3 deliquescence relative humidity (DRH) was first calculated using equation (1) (Eq. 1). The average DRH of NH_4NO_3 between the two sites was 65.0±2.9%, slightly lower than the atmospheric RH (66.0±19.3%). As the works by Wexler and Seinfeld (1991) and Tang and Munkelwitz (1993) revealed, aerosols are multicomponent mixtures, and which the aerosol DRH is always lower than the DRH of the individual salts in the particles. Thus, the actual DRH of the aerosols observed in this study would be lower than the calculated DRH of NH_4NO_3. Based on these analyses, the particles would be deliquescent most of the time, but for simplification, we always assumed that NH_4NO_3 was in an aqueous state, corresponding to the following dissociation reaction (R1):

$$\ln(\mathrm{DRH}) = \frac{723.7}{\mathrm{T}} + 1.6954 \qquad \text{(Eq. 1)}$$

$$\mathrm{NH_3(g) + HNO_3(g) \leftrightarrows NH_4^+ + NO_3^-} \qquad \text{(R1)}$$

According to the approach illustrated in the referenced work (Seinfeld and Johnh,

2016), the equilibrium constant of the dissociation reaction can be described as the equation (2).

$$K_{AN}=\frac{\gamma^2_{NH_4NO_3} m_{NH_4^+} m_{NO_3^-}}{p_{HNO_3} p_{NH_3}} \quad \text{(Eq. 2)}$$

$$K_{AN}=4\times10^{17}\exp\left\{64.7\left(\frac{298}{T}-1\right)+11.51\left[1+\ln\left(\frac{298}{T}\right)-\frac{298}{T}\right]\right\} \quad \text{(Eq. 3)}$$

$$\ln(K_p)=118.7-\frac{24084}{T}-6.025\ln(T) \quad \text{(Eq. 4)}$$

where K_{AN} ($mol^2/(kg^2\ atm^2)$) is the equilibrium constant of R1 (this value is temperature-dependent and can be calculated by Eq. 3), γ_{NH4NO3} is the binary activity coefficient for NH_4NO_3 ($\gamma_{NH4NO3}=\gamma_{NH4}\gamma_{NO3}$), and m_{NH4+} and m_{NO3-} are the molalities of NH_4^+ and NO_3^-, respectively. To calculate γ_{NH4NO3} and $m_{NH4+}m_{NO3-}$, the activity coefficients of the corresponding ions and the aerosol water content were assessed using the E-AIM (IV) model (http://www.aim.env.uea.ac.uk/aim/model4/model4a.php). Combining equations (2) and (3), we obtained the product of the partial pressures of NH_3 and HNO_3 ($P_{HNO3}P_{NH3}$), obtaining an average of ~15.2±26.0 ppb^2 at the MF site. This value was within the range of values (1.0~37.7 ppb^2) measured by the IGAC in the summer of 2017 in Xi'an, a metropolitan city located in the Guanzhong Basin of inland China that has suffered from serious haze pollution (Wu et al., 2020a). Thus, we believe that $P_{HNO3}P_{NH3}$ variations can be assessed using the above method to a certain extent. For simplification, the dissociation constant of dry NH_4NO_3 particle (Kp, ppb^2) was thus applied in this study, which can be calculated as a function of temperature using Eq. 4, as was revealed by Mozurkewich (1993). Despite without considering the aerosol properties (e.g, acidity, mixing state) that may induce the shift of NH_4NO_3 equilibrium states, this assessment method was also applied in the similar work

conducted by Lindaas et al. (2021).

3 Results and discussion

3.1 Overview of $PM_{2.5}$ at both sites

3.1.1 Meteorological conditions and temporal variations in $PM_{2.5}$ concentrations

The temporal variations in the 4-hr $PM_{2.5}$ mass concentrations, water-soluble ions and meteorological factors measured at the two sampling sites are illustrated in Figure 2, and the comparisons of the above variables are summarized in Table 1. The average temperature (T) and relative humidity (RH) at the MF site were 23.2±4.2 °C and 68.9±18.2% (Table 1), respectively, and these values were characterized by marked diurnal variations, as shown in Figure 2a. However, relatively cold and moist weather frequently occurred at the MS site, which exhibited less pronounced diurnal T and RH variations, with variations approximately 8 °C and 6% lower than the mean values derived at the MF site, respectively. Windy weather (wind speed: 3.2±2.0 m/s) also prevailed at this sampling site with gusts above 10.0 m/s; this condition is conducive to the dissipation of pollutants.

Overall, the $PM_{2.5}$ concentrations measured at the MF site varied from 22.8 μg/m^3 to 245.6 μg/m^3, with a mean value of 76.0±44.1 μg/m^3, approximately corresponding to Grade II (75 μg/m^3) of the National Ambient Air Quality Standard in China. Even so, the $PM_{2.5}$ levels at Huashan town (i.e., at the MF site) were still higher than those measured in many typical megacities in the summertime, e.g., Xian (37 μg/m^3 in 2017) (Wu et al., 2020b) and Beijing (46.3 μg/m^3 in 2016) (Lv et al., 2019). Noticeably, stagnant meteorological conditions with increasing RH (> 77%) and

relatively low wind speeds (< 2.0 m/s) occurred during the relatively late stage of observation, leading to a buildup of high $PM_{2.5}$ loadings (78.7 μg/m^3 to 245.6 μg/m^3). Such typical haze events last approximately 4 days (12 September to 16 September, 2016), indicating that aerosol pollution is still severe in rural towns despite the notable air quality improvements recorded in most Chinese urban areas. A similar temporal $PM_{2.5}$ pattern was seen at the MS site, where the average $PM_{2.5}$ concentration (47.0±38.0 μg/m^3) was only 0.62-fold that at the MF site and was within the range of that measured at the summit of Mt. Tai (37.9 μg/m^3 in 2016) (Yi et al., 2021) and on Mt. Lushan (55.9 μg/m^3 in 2011) (Li et al., 2015) in summertime. As shown in Figure 2d, a multiday episode (mean $PM_{2.5}$: 106.3 μg/m^3) also appeared at the MS site during the period from 12 September to 15 September, corresponding to the days on which high surface pollution was recorded. This was indicative of the potential impacts of surface pollution on air quality in mountainous areas.

3.1.2 Diurnal variation in $PM_{2.5}$

As shown in Figure 2c and 2d, regular diurnal $PM_{2.5}$ variations were seen throughout the whole campaign, especially at the MS site. To reveal the differences in the daily changes in $PM_{2.5}$ between the two sampling sites, the mean diurnal cycles of hourly $PM_{2.5}$ and the boundary layer height (BLH) are depicted in Figure 3. At the low-elevation site, the $PM_{2.5}$ concentration was moderately enhanced during the nighttime, with a daily maximum (88.2±53.0 μg/m^3) observed at 6:00 local standard time (LST). After sunrise, $PM_{2.5}$ exhibited a decreasing trend until ~15:00 LST, corresponding to thermally driven boundary-layer growth. Conversely, the aerosol concentrations at the

higher-elevation site immediately increased as the boundary layer uplifted in the early morning and peaked at 14:00 LST, when the MS site was located completely within the interior of the boundary layer. Proverbially, anabatic valley winds prevail in mountainous regions during the daytime. Thus, the aerosol-rich air at MF site may be transported aloft by the prevailing valley breeze, leading to significantly enhanced $PM_{2.5}$ levels at the MS site in short time periods. This finding was further verified by the similar diurnal NO_2 pattern identified at the MS site, as illustrated in Figure S1. In the forenoon period, continuous enhancement in the NO_2 level was observed at the MS site, with a daily maximum of 14.4±53.0 μg/m^3 (at 11:00 LST); this maximum was ~7-fold the early-morning NO_2 concentration. However, O_3 exhibited indistinctive variations during this period, and this was indicative of less NO_2 being generated from photochemical reactions. As mentioned above, there are no obvious anthropogenic emission sources around the MS site; therefore, our observations indicate the remarkable transport of pollutants from the lower ground surface to higher elevations during the daytime.

Moreover, the $PM_{2.5}$ concentrations at the MS site exhibited less nighttime variation, with a modest abatement (Figure 3b). The nocturnal BLH usually remained below the elevation of the MS site; thus, the surface $PM_{2.5}$ may have contributed less to the aerosol levels at the MS site at night. To identify the potential spatial sources of nocturnal $PM_{2.5}$ at the high-elevation site, a high-elevation CWT analysis was conducted. As illustrated in Figure 4, the CWT values in the daylight hours were mostly concentrated over the sampling site, consistent with our above discussions. However, relatively high

317 nighttime CWT loadings were distributed on Mt. Hua and in its surrounding regions,
318 indicating that regional transport may be a major source of $PM_{2.5}$ at the MS site at night.
319 Thus, the constituents of and variations in nocturnal $PM_{2.5}$ at the MS site may be mainly
320 the results of regional features. For verifying the feasibility of vertical transport of air
321 parcel, the WRF-Chem model was applied here to simulate wind filed and the
322 divergence that represents the expansion-rate of the air mass in unit time. From Figure
323 5(a), the southerly winds prevailed at mountain foot area during the whole campaign,
324 which would blow the pollutants into the valley. And these pollutants at low-elevation
325 can be transported to the upper layer by the updrafts as indicated by the positive values
326 of vertical divergence at MF area that decreased with enhanced elevation (Figure 5(b)).
327 Besides that, we also analyzed the organic compounds in $PM_{2.5}$ samples, e.g.,
328 levoglucosan, BkF and IP+BghiP, which are major tracers for the emissions from
329 biomass burning, coal combustion and vehicle exhausts, respectively (Wang et al., 2009;
330 Wu et al., 2020b; Wang et al., 2007). From Figure S2, the indistinctive divergences of
331 diagnostic ratios and proportion of these organic tracers were found among both
332 sampling sites, suggesting an insignificant change of the corresponding emission
333 sources during the transport.

334 **3.2 Characterization of water-soluble ions in $PM_{2.5}$**

335 **3.2.1 Comparisons of water-soluble ions between the two sites**

336 Figure 6 shows the fractional contributions of the chemical compositions to the
337 $PM_{2.5}$ at both sampling sites. As summarized in Table 1, the water-soluble ion level
338 (WSI, 24.0±15.0 $\mu g/m^3$) at lower-elevation site was comparable to that of organic

matter (OM, OM=1.6×OC) (Wang et al., 2016), with a fractional contribution of ~31% to $PM_{2.5}$ (Figure 6). At the higher-elevation site, the WSI exhibited lower values (19.5±16.0 μg/m^3), yet the proportion was moderately enhanced by ~6%. Notably, this elevated contribution of WSIs was mostly attributed to sulfate and ammonium. Similar patterns in which the secondary inorganic ions (sulfate, nitrate and ammonium, (SNA)) mass fraction increased with altitude within the mixing height have also been observed in Terni Valley (central Italy) (Ferrero et al., 2012) and Salt Lake Valley (US) (Baasandorj et al., 2017). Among the SNA components, sulfate was the predominant species, exhibiting slight mass concentration differences between the two sampling sites (10.1±6.4 μg/m^3 versus 9.0±7.1 μg/m^3). However, an ~4% enhancement in the mass fraction of sulfate was measured at the higher elevation. Ammonium also exhibited a similar feature, accounting for ~5%-7.5% of the $PM_{2.5}$. These sulfate and ammonium mass concentration homogeneities across the two sites were indicative of the further formation of these two ions during transport. Unlike sulfate and ammonium, nitrate and its proportions showed opposite trends, decreasing with elevation; this was consistent with most of the measured components. Above variation features of SNA among two sites were found at most of moments in the campaign, except for 12-13 September with a higher SNA concentration at MS site (Figure 2e and 2f). On these two days MS site remained outside the boundary layers (a.s.l., ~550 m), suggesting less effect of the surface pollutants on the aerosol upper layers. While, the precursor masses (~12.3 μg/m^3 for SO_2 and 8.4 μg/m^3 for NO_2) were insufficient to form so much SNA at MS site. Thus, the higher SNA aloft

on above two days may be mostly driven by regional or long-range transport. This can be verified by the CWT analysis, of which high loadings were mainly distributed in the west and southwest areas of Mt. Hua (Figure S3a), and the cities on the air mass transport pathways (e.g., Xi'an and Weinan) also suffered from moderate haze pollution on these two days (Figure S3b). On account of the different sources, the samples during 12-13 September were excluded in the followed discussion. Whereas, the remaindering SNA data still exhibited the similar variations as mentioned above, and the divergence in nitrate mass concentration and fractional contribution to $PM_{2.5}$ among two sites even became more pronounced (Figure S4). Moreover, distinct nitrate size distributions were also observed between the different sites in the summertime of 2020 (Figure S5). From the Figure S5, we can note that the nitrate at low-elevation was enriched in the fine mode with a minor peak in the coarse fraction. However, the high-elevation nitrate exhibited a bimodal pattern with two equivalent peaks in the fine and coarse fractions and was well correlated with coarse mode calcium but poorly correlated with ammonium (R^2=0.51, $p<0.05$). To our knowledge, ammonium nitrate, a major form of fine-mode particulate nitrate, can be easily volatilized and converted into gas-phase NH_3 and HNO_3 (Pakkanen, 1996; Harrison and Pio, 1983). Thus, the gaseous HNO_3 volatilized from fine PM may react with coarse-modal cations (e.g., Ca^{2+}, Mg^{2+} and Na^{+}) to form nonvolatile salts, leading to that significant nitrate shifts from fine particles to large particles. A similar phenomenon was also found in our previous study conducted at the summit of Mt. Hua (Wang et al., 2013). Nonvolatile sulfate was predominantly found in the fine

fraction at both sampling sites, which may support this concept. More evidence for this hypothesis is presented below in section 3.3.

The diurnal cycles of the 4-hr sulfate, nitrate and ammonium are illustrated in Figure S6. As shown in Figure S6, the total SNA concentration at the MF site exhibited a morning peak from 8:00-12:00 LST; this variation was quite different from that of $PM_{2.5}$. Such a difference between the total SNA and $PM_{2.5}$ at the MF site could partially be attributed to the lower sampling resolution and enhanced formation of SNA in the morning. The diurnal total SNA pattern identified at the MS site coincided with the $PM_{2.5}$ pattern, exhibiting a daily maximum reaching ~21.2±19.9 $\mu g/m^3$ (from 12:00-16:00 LST), a 1.2-fold increase compared to that measured at the MF site. Among the SNA components, morning peaks of nitrate and ammonium (from 8:00-12:00 LST) were also observed at the MF site. These nitrate and ammonium at MF site can contribute to that at the MS site through vertical transport, leading to a significant enhancement in nitrate and ammonium concentrations aloft with the afternoon peaks during 12:00-16:00 LST. Even so, the maximum nitrate concentration at the MS site (6.5±7.4 $\mu g/m^3$) was still lower than that measured at the MF site (8.9±6.8 $\mu g/m^3$) due to the NH_4NO_3 volatilization under the transport process, while ammonium exhibited the opposite trend. This finding was consistent with the above discussion. Unlike nitrate and ammonium, similar diurnal variations in sulfate were observed between the two sampling sites, with daily maxima observed from 12:00-16:00 at both sites. The major sulfate formation pathway during the daytime in summer is the photooxidation of SO_2 with an OH radical, and the formation rate

facilitated by this process is much lower than that of the nitrate formation process (Seinfeld and Johnh, 2016; Rodhe et al., 1981). Thus, sulfate formation may occur continuously during vertical transport, leading to smaller difference in the diurnal cycle of sulfate between the two sites.

3.2.2 Chemical forms of SNA at both sites

As shown in Figure 6, the water-soluble ions considered herein mainly included sulfate, nitrate and ammonium, which usually exist in the form of ammonium salts (NH_4HSO_4, $(NH_4)_2SO_4$, NH_4NO_3, and so on). In the H_2SO_4-HNO_3-NH_3 thermodynamic system, H_2SO_4 and HNO_3 are neutralized by ammonia under ammonia-rich conditions and mainly exist as $(NH_4)_2SO_4$ and NH_4NO_3 in aerosols. Conversely, H_2SO_4 is converted to HSO_4^- in environments with relatively low NH_3 availabilities. Thus, NH_4HSO_4 and NH_4NO_3 may be the dominant aerosol components under such environmental conditions (Rodhe et al., 1981; Seinfeld and Johnh, 2016). To reveal the major SNA forms at the different sampling sites considered herein, the theoretical ammonium concentration was calculated according to thermodynamic equilibrium with the atmospheric sulfate and nitrate levels. The theoretical ammonium levels were calculated as follows:

$$NH_{4\,theory}^{+}=\left(\frac{[SO_4^{2-}]}{48}+\frac{[NO_3^{-}]}{62}\right)\times 18 \quad \text{(Eq. 5)}$$

$$NH_{4\,theory}^{+}=\left(\frac{[SO_4^{2-}]}{96}+\frac{[NO_3^{-}]}{62}\right)\times 18 \quad \text{(Eq. 6)}$$

where $[SO_4^{2-}]$ and $[NO_3^{-}]$ represent atmospheric concentrations ($\mu g/m^3$). When $(NH_4)_2SO_4$ and NH_4NO_3 are the dominant species, the $NH_4^{+}{}_{theory}$ can be calculated using equation (5). In contrast, equation (6) suggests that NH_4HSO_4 and NH_4NO_3 are

abundantly present in the analyzed aerosols. Figure 7 compares the measured NH_4^+ concentrations with the theoretical NH_4^+ concentrations derived by the two equations above. As illustrated in Figure 7(a), the slope of the observational NH_4^+ values against the theoretical NH_4^+ values calculated using equation (6) was much closer to one at the MF site than at the MS site, meaning that NH_4HSO_4 and NH_4NO_3 were the major chemical forms of SNA at MF site. However, the opposite pattern was revealed at the higher-elevation site; thus, the upper aerosols were characterized by abundant $(NH_4)_2SO_4$ and NH_4NO_3. Based on observational data collected during the 2020 summertime, the ammonia level at MF site (36.0±68.0 ppb) was ~9-fold that at MS site (4.1±2.5 ppb). Under such abundant ammonia environment, the S(VI) was in the major form of NH_4HSO_4 but $(NH_4)_2SO_4$ in relatively low ammonia environment, which was somewhat unexpected. As can be inferred from earlier studies (Seinfeld and Johnh, 2016; Shi et al., 1999), the ammonia Henry's law coefficients generally increase in value as the temperature decreases. Therefore, the lower temperatures measured at the MS site would create a more favorable environment for ammonia, thus shifting its partitioning toward the particulate phase. The HSO_4^- transported from the MF site would thus be further neutralized to SO_4^{2-} by this additional ammonium during transport, leading to the significant difference observed in the chemical forms of SNA between the two sites. Moreover, as the chemical component change from NH_4HSO_4 to $(NH_4)_2SO_4$, the aerosol acidity moderately decreased, showing a higher bulk $PM_{2.5}$ pH (3.4±2.2) at relatively clean upper layer and a lower value (2.9±2.0) at heavily polluted grounds (Table 1). However, the previous studies were generally recognized

447 that the aerosol would become more acidic when the air parcels were transported from
448 the polluted to cleaner/remote regions (Liu et al., 1996; Nault et al., 2021). As shown
449 in Table 1, the change in aerosol liquid water content (ALWC) has an indistinctive
450 difference among both sampling sites (*t*-test, $p>0.05$). Thus, we think that such a
451 reduced aerosol acidity with increasing elevation in our study was mainly due to the
452 change in chemical component, which was caused by the different physicochemical
453 behaviors of the semi-volatile species nitrate and ammonium during transport. More
454 discussions are included in the following section.

455 **3.3 Physicochemical behaviors of nitrate and ammonium during transport**

456 According to the above discussion, a conceptual model illustrating the
457 physicochemical behaviors of nitrate and ammonium during vertical transport was
458 proposed to explain the chemical composition differences between the two sites. As
459 shown in Figure 8, surface air parcels containing abundant NH_4HSO_4 and NH_4NO_3
460 particles can be transported to the upper atmosphere by the prevailing valley winds,
461 and during this process, the volatile NH_4NO_3 is easily converted to gaseous NH_3 and
462 HNO_3. Subsequently, heterogeneous reactions of the gaseous HNO_3 with fugitive dust
463 occur, thus forming nonvolatile salts and resulting in the accumulation of nitrate on
464 the coarse-mode particles. However, as the temperature decreased, the ammonia that
465 volatilized from the fine particles or was derived from the surface can re-enter the
466 particulate phase through the gas–particle partition. Therefore, $(NH_4)_2SO_4$ would be
467 formed in the aerosol phase and would gradually replace NH_4HSO_4.

468 To investigate the likelihood of NH_4NO_3 volatilization during the transport process,

the dissociation constant of NH_4NO_3 (Kp) and the partial pressures of gas-phase NH_3 and HNO_3 were calculated in this study. More details regarding the calculation steps of the above factors can be found in section 2.4. Based on the thermodynamic principles presented by Stelson and Seinfeld (1982), when the product of the partial pressures of NH_3 and HNO_3 ($P_{HNO3}\times P_{NH3}$) is greater than Kp, the equilibrium of the system shifts toward the aerosol phase, thus increasing NH_4NO_3 formation. In contrast, a relatively low $P_{HNO3}\times P_{NH3}$/Kp value (<1) suggests that NH_4NO_3 dissociation is induced and that NH_4NO_3 is transferred to the gas phase. Figure 9 depicts the ratio of the product of the partial pressures of NH_3 and HNO_3 with different ambient temperatures. As shown in Figure 9, approximately 85% of the samples collected at both sampling sites were located within the region with $P_{HNO3}\times P_{NH3}$/Kp less than 1, demonstrating a common NH_4NO_3 dissociation phenomenon during the observed period. For the samples with $P_{HNO3}\times P_{NH3}$/Kp ratios <1, the mean value of the MS-site ratios was approximately half that of the MF-site ratios, indicating that NH_4NO_3 dissociation may be more likely at higher elevations than that at lower elevations. This finding was inconsistent with the aircraft observations of the wildfire smoke plumes collected by Lindaas et al. (2021), who revealed that $P_{HNO3}\times P_{NH3}$/Kp exhibited an increasing trend within 1-3 km (a.s.l.). As we know, the abundant NH_3 and NO*x* can be emitted by the wildfire, which would be transported aloft and lead to a higher NH_3 and HNO_3 mixing ratio compared to that at lower elevation. This drive a higher $P_{HNO3}\times P_{NH3}$/Kp ratio at the upper layers of aircraft observations in the western U.S. (Lindaas et al., 2021).

Moreover, the nitrogen isotope compositions of nitrate and ammonium in $PM_{2.5}$ that can retain invaluable information regarding physicochemical processes (Wiedenhaus et al., 2021; Elliott et al., 2019), were thus measured to further verify the conceptual model. As previously mentioned, unlike daytime pollutants, nocturnal pollutants exhibited different sources between the two sampling sites. Thus, their nitrogen isotope compositions were more complicated and less comparable. However, for simplicity, only the daytime samples were analyzed herein based on the hypothesis that the sources of the high-elevation pollutants were the same as those of the pollutants collected at the MF site. As shown in Figure 10, a discrepancy in the $\delta^{15}N$ value of nitrate ($\delta^{15}N\text{-}NO_3^-$) featuring more ^{15}N-enriched NO_3^- was observed at the higher elevation, with a *p* value less than 0.05. This finding can be ascribed to the evaporation of a portion of the particulate NH_4NO_3 due to a dissociation shift in equilibrium; in this shift, the lighter ^{14}N was preferentially incorporated into the atmosphere, leading to ^{15}N enrichment in the remaining nitrate. Similar phenomenon was also revealed by Wiedenhaus et al. (2021), who thought that the ammonium nitrate dissociation may be an important reason for the accumulation of ^{15}N in aerosol particles. Additionally, Freyer et al. (1993) revealed that gas-phase isotopic exchanges between NO and NO_2 result in the enrichment of the heavier ^{15}N isotope in the more oxidized form and may further affect $\delta^{15}N\text{-}NO_3^-$ through nitrate formation reactions. The above isotopic exchange between NO_2 and NO*x* can be roughly described as follows: $[\delta^{15}N(NO_2)\text{-}\delta^{15}N(NOx)]=(1\text{-}K)\times(1\text{-}f_{NO2})$, where *K* and f_{NO2} are the temperature-dependent exchange constant and mole fraction of NO_2, respectively.

Based on trace gas observations, the f_{NO2} values of the air aloft were very high due to the frequently undetectable NO concentration, indicating a rather limited isotopic exchange between NO_2 and NO. Therefore, the evaporation of particulate NH_4NO_3 have been the significant factor affecting the measurement of a higher $\delta^{15}N\text{-}NO_3^-$ at the MS site than at the MF site in our observations. According to the above analysis, the ammonium at higher elevation should theoretically be more and more enriched in $\delta^{15}N$ with the continuous NH_4NO_3 volatilization. However, our observation of $\delta^{15}N\text{-}NH_4^+$ did not correspond to above pattern, namely, ammonium at the MS site depleted in $\delta^{15}N$ compared to that at MF site ($p<0.05$, Figure 10). Given the unchanged ammonia sources, such seemingly unreasonable observations were mainly caused by the gas-to-particle conversion of ammonia. In this process, the reversible phase-equilibrium reactions between $NH_3(g)$ and $HNO_3(g)/HCl(g)$ would yield positive enrichment in $\delta^{15}N$ of aerosol NH_4^+ (Walters et al., 2019); nevertheless, unidirectional reactions involving $NH_3(g)$ and SO_4^{2-}/HSO_4^- favored ^{15}N depletion in the particle form as revealed by Heaton et al. (1997). Thereby, the lower $\delta^{15}N\text{-}NH_4^+$ values at MS site were mostly driven by those irreversible reactions, rather than the reversible equilibrium ones. This result further confirmed our conjecture that the additional ammonia would partition into particulate phases and further neutralize the acidic NH_4HSO_4, leading to an increasing pH at MS site compared to that at MF site. Taken together, this compelling evidence verifies that fine-mode nitrate and ammonium exhibit distinctly different physicochemical behaviors during their transport.

4 Conclusions and atmospheric implications

In this study, aerosol samples were collected at 4-hr intervals on the mountainside of Mt. Hua, and the OC, EC, water-soluble ions and isotope compositions of nitrate and ammonium were measured and compared with simultaneous observations taken at a lower-elevation site (MF site). The particle mass at the MF site was approximately 1.5-fold that at the higher elevation, and distinctly different diurnal cycles were observed between the two sampling sites. Based on the BLH variation, we revealed that near-surface $PM_{2.5}$ could be transported to the upper layers by the mountain-valley breeze, leading to the gradual accumulation of pollutants on the mountainside during the daytime.

Sulfate, the predominant species found among ions at both sampling sites, exhibited nearly identical mass concentrations at the two sites but had a moderately enhanced mass fraction at the higher elevation. Such homogeneity was also observed in ammonium, which mainly existed as NH_4HSO_4+NH_4NO_3 and $(NH_4)_2SO_4$+NH_4NO_3 at the lower- and higher-elevation sites, respectively. This observation indicated the further formation of ammonium during the transport process. Unlike sulfate and ammonium, nitrate at the MS site exhibited abated trends in both its concentration and proportion, mainly due to the volatilization of NH_4NO_3. With the help of nitrate and ammonium nitrogen isotopes, we proposed a conceptual model to illustrate the different behaviors of nitrate and ammonium during vertical transport; in this model, the semivolatile NH_4NO_3 in surface air parcels was easily converted into gaseous NH_3 and HNO_3. Subsequently, heterogeneous reactions occurred between this gaseous HNO_3 and fugitive dust, forming nonvolatile salts and

leading to a significant nitrate shift from fine particles into coarse particles. In addition, the decreasing temperature was favorable for ammonia partitioning toward the particle phase, and the addition of ammonium further neutralized HSO_4^- to form SO_4^{2-}. This process would reduce the aerosol acidity, with bulk $PM_{2.5}$ pH increasing from 2.9±2.0 at MF site to 3.4±2.2 at MS site.

Over the past decade, the relative abundance of NH_4NO_3 has been enhanced in most urban areas of China because strict emission directives have been promulgated to abate the emission and environmental impacts of SO_2 (Xie et al., 2020; Song et al., 2019). In this work, we observed that NH_4NO_3 volatilization was a ubiquitous phenomenon for particles during transport, resulting in a shift in partwise nitrate from the fine mode to the coarse fraction; this shift has also been reported in the offshore areas of the UK (Yeatman et al., 2001). Thus, we think that considering only fine-fraction nitrate may result in the conversion rate of NO*x* to nitrate being partly underestimated at some times, especially in the summer. Moreover, the deposition velocity of coarse particles is usually faster than that of fine particles; therefore, the above process would appreciably elevate the deposition of N into the environment. Indeed, abundant NO_2, O_3 and NH_3 co-occurrence is common in the East Asian atmosphere, and under these conditions, secondary inorganic aerosols can be effectively produced, leading to a $PM_{2.5}$ loading explosion in the urban atmosphere of China (Wu et al., 2020c; Wang et al., 2016). Given this, harmonious reductions in NO_2, O_3 and NH_3 will be urgent in further mitigation strategies to improve air quality and alleviate other potential effects.

Author contributions. GW designed the experiment. CW, JiaL and CC collected the samples. CW and CC conducted the experiments. CW and GW performed the data interpretation and wrote the paper. All authors contributed to the paper with useful scientific discussions or comments.

Competing interests. The authors declare that they have no conflict of interest.

Acknowledgements. This work was financially supported by the National Natural Science Foundation of China (No. 42130704, 42007202), Shanghai Science and Technology Innovation Action Plan (20dz1204000) and ECNU Happiness Flower program. We thank Lang Liu from School of Public Policy and Administration, Northwestern Polytechnical University, Xi'an, China for him support of model simulation in meteorological data during the campaign.

References

Andreae, M. O. and Ramanathan, V.: Climate's Dark Forcings, Science, 340, 280-281, 10.1126/science.1235731, 2013.

Baasandorj, M., Hoch, S. W., Bares, R., Lin, J. C., Brown, S. S., Millet, D. B., Martin, R., Kelly, K., Zarzana, K. J., Whiteman, C. D., Dube, W. P., Tonnesen, G., Jaramillo, I. C., and Sohl, J.: Coupling between Chemical and Meteorological Processes under Persistent Cold-Air Pool Conditions: Evolution of Wintertime PM2.5 Pollution Events and N2O5 Observations in Utah's Salt Lake Valley, Environ. Sci. Technol., 51, 5941-5950, 10.1021/acs.est.6b06603, 2017.

Bond, T. C., Doherty, S. J., Fahey, D. W., Forster, P. M., Berntsen, T., DeAngelo, B. J., Flanner, M. G., Ghan, S., Kaercher, B., Koch, D., Kinne, S., Kondo, Y., Quinn, P. K., Sarofim, M. C., Schultz, M. G., Schulz, M., Venkataraman, C., Zhang, H., Zhang, S., Bellouin, N., Guttikunda, S. K., Hopke, P. K., Jacobson, M. Z., Kaiser, J. W., Klimont, Z., Lohmann, U., Schwarz, J. P., Shindell, D., Storelvmo, T., Warren, S. G., and Zender, C. S.: Bounding the role of black carbon in the climate system: A

609 scientific assessment, J. Geophys. Res.-Atmos., 118, 5380-5552, 10.1002/jgrd.50171, 2013.
610 Carslaw, K. S., Lee, L. A., Reddington, C. L., Pringle, K. J., Rap, A., Forster, P. M., Mann, G. W.,
611 Spracklen, D. V., Woodhouse, M. T., Regayre, L. A., and Pierce, J. R.: Large contribution of natural
612 aerosols to uncertainty in indirect forcing, Nat., 503, 67-+, 10.1038/nature12674, 2013.
613 Dzepina, K., Mazzoleni, C., Fialho, P., China, S., Zhang, B., Owen, R. C., Helmig, D., Hueber, J., Kumar,
614 S., Perlinger, J. A., Kramer, L. J., Dziobak, M. P., Ampadu, M. T., Olsen, S., Wuebbles, D. J., and
615 Mazzoleni, L. R.: Molecular characterization of free tropospheric aerosol collected at the Pico
616 Mountain Observatory: a case study with a long-range transported biomass burning plume, Atmos.
617 Chem. Phys., 15, 5047-5068, 10.5194/acp-15-5047-2015, 2015.
618 Elliott, E. M., Yu, Z., Cole, A. S., and Coughlin, J. G.: Isotopic advances in understanding reactive
619 nitrogen deposition and atmospheric processing, Sci. Total Environ., 662, 393-403,
620 10.1016/j.scitotenv.2018.12.177, 2019.
621 Fan, J., Rosenfeld, D., Zhang, Y., Giangrande, S. E., Li, Z., Machado, L. A. T., Martin, S. T., Yang, Y.,
622 Wang, J., Artaxo, P., Barbosa, H. M. J., Braga, R. C., Comstock, J. M., Feng, Z., Gao, W., Gomes,
623 H. B., Mei, F., Poehlker, C., Poehlker, M. L., Poeschl, U., and de Souza, R. A. F.: Substantial
624 convection and precipitation enhancements by ultrafine aerosol particles, Science, 359, 411-+,
625 10.1126/science.aan8461, 2018.
626 Fan, M.-Y., Zhang, Y.-L., Lin, Y.-C., Hong, Y., Zhao, Z.-Y., Xie, F., Du, W., Cao, F., Sun, Y., and Fu, P.:
627 Important Role of NO3 Radical to Nitrate Formation Aloft in Urban Beijing: Insights from Triple
628 Oxygen Isotopes Measured at the Tower, Environ. Sci. Technol., 10.1021/acs.est.1c02843, 2021.
629 Fang, Y. T., Koba, K., Wang, X. M., Wen, D. Z., Li, J., Takebayashi, Y., Liu, X. Y., and Yoh, M.:
630 Anthropogenic imprints on nitrogen and oxygen isotopic composition of precipitation nitrate in a
631 nitrogen-polluted city in southern China, Atmos. Chem. Phys., 11, 1313-1325, 10.5194/acp-11-
632 1313-2011, 2011.
633 Ferrero, L., Cappelletti, D., Moroni, B., Sangiorgi, G., Perrone, M. G., Crocchianti, S., and Bolzacchini,
634 E.: Wintertime aerosol dynamics and chemical composition across the mixing layer over basin
635 valleys, Atmos. Environ., 56, 143-153, 10.1016/j.atmosenv.2012.03.071, 2012.
636 Freyer, H. D., Kley, D., Volz-Thomas, A., and Kobel, K.: On the interaction of isotopic exchange
637 processes with photochemical reactions in atmospheric oxides of nitrogen, Journal of Geophysical
638 Research, 98, 14791-14796, 10.1029/93jd00874, 1993.
639 Fuzzi, S., Baltensperger, U., Carslaw, K., Decesari, S., van der Gon, H. D., Facchini, M. C., Fowler, D.,
640 Koren, I., Langford, B., Lohmann, U., Nemitz, E., Pandis, S., Riipinen, I., Rudich, Y., Schaap, M.,
641 Slowik, J. G., Spracklen, D. V., Vignati, E., Wild, M., Williams, M., and Gilardoni, S.: Particulate
642 matter, air quality and climate: lessons learned and future needs, Atmos. Chem. Phys., 15, 8217-
643 8299, 10.5194/acp-15-8217-2015, 2015.
644 Guo, S., Hu, M., Zamora, M. L., Peng, J., Shang, D., Zheng, J., Du, Z., Wu, Z., Shao, M., Zeng, L.,
645 Molina, M. J., and Zhang, R.: Elucidating severe urban haze formation in China, Proc. Natl. Acad.
646 Sci. USA, 111, 17373-17378, 10.1073/pnas.1419604111, 2014.
647 Harrison, R. M. and Pio, C. A.: Size-differentiated composition of inorganic atmospheric aerosols of both
648 marine and polluted continental origin, Atmos. Environ., 17, 1733-1738, 10.1016/0004-
649 6981(83)90180-4, 1983.
650 Heaton, T. H. E., Spiro, B., Madeline, S., and Robertson, C.: Potential canopy influences on the isotopic
651 composition of nitrogen and sulphur in atmospheric deposition, Oecologia, 109, 600-607,
652 10.1007/s004420050122, 1997.

Lambey, V. and Prasad, A. D.: A Review on Air Quality Measurement Using an Unmanned Aerial Vehicle, Water, Air, & Soil Pollution, 232, 10.1007/s11270-020-04973-5, 2021.

Lelieveld, J., Evans, J. S., Fnais, M., Giannadaki, D., and Pozzer, A.: The contribution of outdoor air pollution sources to premature mortality on a global scale, Nat., 525, 367-+, 10.1038/nature15371, 2015.

Li, D., Wu, C., Zhang, S., Lei, Y., Lv, S., Du, W., Liu, S., Zhang, F., Liu, X., Liu, L., Meng, J., Wang, Y., Gao, J., and Wang, G.: Significant coal combustion contribution to water-soluble brown carbon during winter in Xingtai, China: Optical properties and sources, J. Environ. Sci., 124, 892-900, 10.1016/j.jes.2022.02.026, 2023.

Li, J. J., Wang, G. H., Cao, J. J., Wang, X. M., and Zhang, R. J.: Observation of biogenic secondary organic aerosols in the atmosphere of a mountain site in central China: temperature and relative humidity effects, Atmos. Chem. Phys., 13, 11535-11549, 10.5194/acp-13-11535-2013, 2013.

Li, T., Wang, Y., Li, W. J., Chen, J. M., Wang, T., and Wang, W. X.: Concentrations and solubility of trace elements in fine particles at a mountain site, southern China: regional sources and cloud processing, Atmos. Chem. Phys., 15, 8987-9002, 10.5194/acp-15-8987-2015, 2015.

Li, W., Shao, L., Zhang, D., Ro, C.-U., Hu, M., Bi, X., Geng, H., Matsuki, A., Niu, H., and Chen, J.: A review of single aerosol particle studies in the atmosphere of East Asia: morphology, mixing state, source, and heterogeneous reactions, Journal of Cleaner Production, 112, 1330-1349, 10.1016/j.jclepro.2015.04.050, 2016.

Lindaas, J., Pollack, I. B., Calahorrano, J. J., O'Dell, K., Garofalo, L. A., Pothier, M. A., Farmer, D. K., Kreidenweis, S. M., Campos, T., Flocke, F., Weinheimer, A. J., Montzka, D. D., Tyndall, G. S., Apel, E. C., Hills, A. J., Hornbrook, R. S., Palm, B. B., Peng, Q., Thornton, J. A., Permar, W., Wielgasz, C., Hu, L., Pierce, J. R., Collett, J. L., Jr., Sullivan, A. P., and Fischer, E. V.: Empirical Insights Into the Fate of Ammonia in Western US Wildfire Smoke Plumes, J. Geophys. Res.-Atmos., 126, 10.1029/2020jd033730, 2021.

Liu, D., Fang, Y., Tu, Y., and Pan, Y.: Chemical Method for Nitrogen Isotopic Analysis of Ammonium at Natural Abundance, Anal. Chem., 86, 3787-3792, 10.1021/ac403756u, 2014.

Liu, L. J. S., Burton, R., Wilson, W. E., and Koutrakis, P.: Comparison of aerosol acidity in urban and semirural environments, Atmos. Environ., 30, 1237-1245, 10.1016/1352-2310(95)00438-6, 1996.

Liu, T., Chan, A. W. H., and Abbatt, J. P. D.: Multiphase Oxidation of Sulfur Dioxide in Aerosol Particles: Implications for Sulfate Formation in Polluted Environments, Environ. Sci. Technol., 55, 4227-4242, 10.1021/acs.est.0c06496, 2021.

Lv, D., Chen, Y., Zhu, T., Li, T., Shen, F., Li, X., and Mehmood, T.: The pollution characteristics of PM10 and PM2.5 during summer and winter in Beijing, Suning and Islamabad, Atmospheric Pollution Research, 10, 1159-1164, 10.1016/j.apr.2019.01.021, 2019.

Lv, S., Wang, F., Wu, C., Chen, Y., Liu, S., Zhang, S., Li, D., Du, W., Zhang, F., Wang, H., Huang, C., Fu, Q., Duan, Y., and Wang, G.: Gas-to-Aerosol Phase Partitioning of Atmospheric Water-Soluble Organic Compounds at a Rural Site in China: An Enhancing Effect of NH3 on SOA Formation, Environ. Sci. Technol., 56, 3915-3924, 10.1021/acs.est.1c06855, 2022.

Meng, J., Wang, G., Hou, Z., Liu, X., Wei, B., Wu, C., Cao, C., Wang, J., Li, J., Cao, J., Zhang, E., Dong, J., Liu, J., Ge, S., and Xie, Y.: Molecular distribution and stable carbon isotopic compositions of dicarboxylic acids and related SOA from biogenic sources in the summertime atmosphere of Mt. Tai in the North China Plain, Atmos. Chem. Phys., 18, 15069-15086, 10.5194/acp-18-15069-2018, 2018.

Mozurkewich, M.: The dissociation constant of ammonium nitrate and its dependence on temperature, relative humidity and particle size, Atmospheric Environment. Part A. General Topics, 27, 261-270, 1993.

Nault, B. A., Campuzano-Jost, P., Day, D. A., Jo, D. S., Schroder, J. C., Allen, H. M., Bahreini, R., Bian, H., Blake, D. R., Chin, M., Clegg, S. L., Colarco, P. R., Crounse, J. D., Cubison, M. J., DeCarlo, P. F., Dibb, J. E., Diskin, G. S., Hodzic, A., Hu, W., Katich, J. M., Kim, M. J., Kodros, J. K., Kupc, A., Lopez-Hilfiker, F. D., Marais, E. A., Middlebrook, A. M., Andrew Neuman, J., Nowak, J. B., Palm, B. B., Paulot, F., Pierce, J. R., Schill, G. P., Scheuer, E., Thornton, J. A., Tsigaridis, K., Wennberg, P. O., Williamson, C. J., and Jimenez, J. L.: Chemical transport models often underestimate inorganic aerosol acidity in remote regions of the atmosphere, Communications Earth & Environment, 2, 10.1038/s43247-021-00164-0, 2021.

Pakkanen, T. A.: Study of formation of coarse particle nitrate aerosol, Atmos. Environ., 30, 2475-2482, 10.1016/1352-2310(95)00492-0, 1996.

Petit, J. E., Favez, O., Albinet, A., and Canonaco, F.: A user-friendly tool for comprehensive evaluation of the geographical origins of atmospheric pollution: Wind and trajectory analyses, Environmental Modelling & Software, 88, 183-187, 10.1016/j.envsoft.2016.11.022, 2017.

Raes, F., Van Dingenen, R., Vignati, E., Wilson, J., Putaud, J. P., Seinfeld, J. H., and Adams, P.: Formation and cycling of aerosols in the global troposphere, Atmos. Environ., 34, 4215-4240, 10.1016/s1352-2310(00)00239-9, 2000.

Reid, J. S., Kuehn, R. E., Holz, R. E., Eloranta, E. W., Kaku, K. C., Kuang, S., Newchurch, M. J., Thompson, A. M., Trepte, C. R., Zhang, J., Atwood, S. A., Hand, J. L., Holben, B. N., Minnis, P., and Posselt, D. J.: Ground-based High Spectral Resolution Lidar observation of aerosol vertical distribution in the summertime Southeast United States, J. Geophys. Res.-Atmos., 122, 2970-3004, 10.1002/2016jd025798, 2017.

rganization, W. H.: WHO global air quality guidelines: particulate matter (PM2. 5 and PM10), ozone, nitrogen dioxide, sulfur dioxide and carbon monoxide, World Health Organization2021.

Rodhe, H., Crutzen, P., and Vanderpol, A.: Formation of sulfuric and nitric acid in the atmosphere during long-range transport, Tellus, 33, 132-141, 1981.

Seinfeld and JohnH: Atmospheric chemistry and physics : from air pollution to climate change / 3nd ed, Atmospheric chemistry and physics : from air pollution to climate change / 3nd ed2016.

Shi, Q., Davidovits, P., Jayne, J. T., Worsnop, D. R., and Kolb, C. E.: Uptake of gas-phase ammonia. 1. Uptake by aqueous surfaces as a function of pH, J. Phys. Chem. A, 103, 8812-8823, 10.1021/jp991696p, 1999.

Shiraiwa, M., Ueda, K., Pozzer, A., Lammel, G., Kampf, C. J., Fushimi, A., Enami, S., Arangio, A. M., Froehlich-Nowoisky, J., Fujitani, Y., Furuyama, A., Lakey, P. S. J., Lelieveld, J., Lucas, K., Morino, Y., Poeschl, U., Takaharna, S., Takami, A., Tong, H., Weber, B., Yoshino, A., and Sato, K.: Aerosol Health Effects from Molecular to Global Scales, Environ. Sci. Technol., 51, 13545-13567, 10.1021/acs.est.7b04417, 2017.

Song, S., Nenes, A., Gao, M., Zhang, Y., Liu, P., Shao, J., Ye, D., Xu, W., Lei, L., Sun, Y., Liu, B., Wang, S., and McElroy, M. B.: Thermodynamic Modeling Suggests Declines in Water Uptake and Acidity of Inorganic Aerosols in Beijing Winter Haze Events during 2014/2015-2018/2019, Environmental Science & Technology Letters, 6, 752-760, 10.1021/acs.estlett.9b00621, 2019.

Stelson, A. W. and Seinfeld, J. H.: Relative humidity and temperature dependence of the ammonium nitrate dissociation constant, Atmos. Environ., 16, 983-992, 10.1016/0004-6981(82)90184-6, 1982.

Tang, I. N. and Munkelwitz, H. R.: Composition and temperature dependence of the deliquescence properties of hygroscopic aerosols, Atmos. Environ., 27, 467-473, 1993.

van Donkelaar, A., Martin, R. V., Brauer, M., Hsu, N. C., Kahn, R. A., Levy, R. C., Lyapustin, A., Sayer, A. M., and Winker, D. M.: Global Estimates of Fine Particulate Matter using a Combined Geophysical-Statistical Method with Information from Satellites, Models, and Monitors, Environ. Sci. Technol., 50, 3762-3772, 10.1021/acs.est.5b05833, 2016.

Walters, W. W., Chai, J., and Hastings, M. G.: Theoretical Phase Resolved Ammonia-Ammonium Nitrogen Equilibrium Isotope Exchange Fractionations: Applications for Tracking Atmospheric Ammonia Gas-to-Particle Conversion, ACS Earth Space Chem., 3, 79-89, 10.1021/acsearthspacechem.8b00140, 2019.

Wang, G., Kawamura, K., Hatakeyama, S., Takami, A., Li, H., and Wang, W.: Aircraft measurement of organic aerosols over China, Environ. Sci. Technol., 41, 3115-3120, 10.1021/es062601h, 2007.

Wang, G., Kawamura, K., Xie, M., Hu, S., Gao, S., Cao, J., An, Z., and Wang, Z.: Size-distributions of n-alkanes, PAHs and hopanes and their sources in the urban, mountain and marine atmospheres over East Asia, Atmos. Chem. Phys., 9, 8869-8882, 10.5194/acp-9-8869-2009, 2009.

Wang, G., Kawamura, K., Xie, M., Hu, S., Li, J., Zhou, B., Cao, J., and An, Z.: Selected water-soluble organic compounds found in size-resolved aerosols collected from urban, mountain and marine atmospheres over East Asia, Tellus Series B-Chemical and Physical Meteorology, 63, 371-381, 10.1111/j.1600-0889.2011.00536.x, 2011.

Wang, G., Zhang, R., Gomez, M. E., Yang, L., Zamora, M. L., Hu, M., Lin, Y., Peng, J., Guo, S., Meng, J., Li, J., Cheng, C., Hu, T., Ren, Y., Wang, Y., Gao, J., Cao, J., An, Z., Zhou, W., Li, G., Wang, J., Tian, P., Marrero-Ortiz, W., Secrest, J., Du, Z., Zheng, J., Shang, D., Zeng, L., Shao, M., Wang, W., Huang, Y., Wang, Y., Zhu, Y., Li, Y., Hu, J., Pan, B., Cai, L., Cheng, Y., Ji, Y., Zhang, F., Rosenfeld, D., Liss, P. S., Duce, R. A., Kolb, C. E., and Molina, M. J.: Persistent sulfate formation from London Fog to Chinese haze, Proc. Natl. Acad. Sci. USA, 113, 13630-13635, 10.1073/pnas.1616540113, 2016.

Wang, G. H., Zhou, B. H., Cheng, C. L., Cao, J. J., Li, J. J., Meng, J. J., Tao, J., Zhang, R. J., and Fu, P. Q.: Impact of Gobi desert dust on aerosol chemistry of Xi'an, inland China during spring 2009: differences in composition and size distribution between the urban ground surface and the mountain atmosphere, Atmos. Chem. Phys., 13, 819-835, 10.5194/acp-13-819-2013, 2013.

Wankel, S. D., Chen, Y., Kendall, C., Post, A. F., and Paytan, A.: Sources of aerosol nitrate to the Gulf of Aqaba: Evidence from delta N-15 and delta O-18 of nitrate and trace metal chemistry, Mar. Chem., 120, 90-99, 10.1016/j.marchem.2009.01.013, 2010.

Wexler, A. S. and Seinfeld, J. H.: Second-generation inorganic aerosol model, Atmos. Environ., 25A, 2731-2748, 1991.

Wiedenhaus, H., Ehrnsperger, L., Klemm, O., and Strauss, H.: Stable N-15 isotopes in fine and coarse urban particulate matter, Aerosol Sci. Technol., 55, 859-870, 10.1080/02786826.2021.1905150, 2021.

Wu, C., Liu, L., Wang, G., Zhang, S., Li, G., Lv, S., Li, J., Wang, F., Meng, J., and Zeng, Y.: Important contribution of N2O5 hydrolysis to the daytime nitrate in Xi'an, China during haze periods: Isotopic analysis and WRF-Chem model simulation, Environmental pollution (Barking, Essex : 1987), 288, 117712-117712, 10.1016/j.envpol.2021.117712, 2021.

Wu, C., Wang, G., Li, J., Li, J., Cao, C., Ge, S., Xie, Y., Chen, J., Liu, S., Du, W., Zhao, Z., and Cao, F.: Non-agricultural sources dominate the atmospheric NH3 in Xi'an, a megacity in the semi-arid region

of China, Sci. Total Environ., 722, 137756, 10.1016/j.scitotenv.2020.137756, 2020a.

Wu, C., Wang, G., Li, J., Li, J., Cao, C., Ge, S., Xie, Y., Chen, J., Li, X., Xue, G., Wang, X., Zhao, Z., and Cao, F.: The characteristics of atmospheric brown carbon in Xi'an, inland China: sources, size distributions and optical properties, Atmos. Chem. Phys., 20, 2017-2030, 10.5194/acp-20-2017-2020, 2020b.

Wu, C., Zhang, S., Wang, G., Lv, S., Li, D., Liu, L., Li, J., Liu, S., Du, W., Meng, J., Qiao, L., Zhou, M., Huang, C., and Wang, H.: Efficient Heterogeneous Formation of Ammonium Nitrate on the Saline Mineral Particle Surface in the Atmosphere of East Asia during Dust Storm Periods, Environ. Sci. Technol., 54, 15622-15630, 10.1021/acs.est.0c04544, 2020c.

Xie, Y., Wang, G., Wang, X., Chen, J., Chen, Y., Tang, G., Wang, L., Ge, S., Xue, G., Wang, Y., and Gao, J.: Nitrate-dominated PM2.5 and elevation of particle pH observed in urban Beijing during the winter of 2017, Atmos. Chem. Phys., 20, 5019-5033, 10.5194/acp-20-5019-2020, 2020.

Xu, Z., Huang, X., Nie, W., Shen, Y., Zheng, L., Xie, Y., Wang, T., Ding, K., Liu, L., Zhou, D., Qi, X., and Ding, A.: Impact of Biomass Burning and Vertical Mixing of Residual-Layer Aged Plumes on Ozone in the Yangtze River Delta, China: A Tethered-Balloon Measurement and Modeling Study of a Multiday Ozone Episode, J. Geophys. Res.-Atmos., 123, 11786-11803, 10.1029/2018jd028994, 2018.

Yeatman, S. G., Spokes, L. J., Dennis, P. F., and Jickells, T. D.: Can the study of nitrogen isotopic composition in size-segregated aerosol nitrate and ammonium be used to investigate atmospheric processing mechanisms?, Atmos. Environ., 35, 1337-1345, 10.1016/s1352-2310(00)00457-x, 2001.

Yi, Y., Meng, J., Hou, Z., Wang, G., Zhou, R., Li, Z., Li, Y., Chen, M., Liu, X., Li, H., and Yan, L.: Contrasting compositions and sources of organic aerosol markers in summertime PM(2.5)from urban and mountainous regions in the North China Plain, Sci. Total Environ., 766, 10.1016/j.scitotenv.2020.144187, 2021.

Zhang, Y., Forrister, H., Liu, J., Dibb, J., Anderson, B., Schwarz, J. P., Perring, A. E., Jimenez, J. L., Campuzano-Jost, P., Wang, Y., Nenes, A., and Weber, R. J.: Top-of-atmosphere radiative forcing affected by brown carbon in the upper troposphere, Nat. Geosci., 10, 486-+, 10.1038/ngeo2960, 2017.

Zheng, B., Tong, D., Li, M., Liu, F., Hong, C., Geng, G., Li, H., Li, X., Peng, L., Qi, J., Yan, L., Zhang, Y., Zhao, H., Zheng, Y., He, K., and Zhang, Q.: Trends in China's anthropogenic emissions since 2010 as the consequence of clean air actions, Atmos. Chem. Phys., 18, 14095-14111, 10.5194/acp-18-14095-2018, 2018.

Zhou, S., Wu, L., Guo, J., Chen, W., Wang, X., Zhao, J., Cheng, Y., Huang, Z., Zhang, J., Sun, Y., Fu, P., Jia, S., Tao, J., Chen, Y., and Kuang, J.: Measurement report: Vertical distribution of atmospheric particulate matter within the urban boundary layer in southern China - size-segregated chemical composition and secondary formation through cloud processing and heterogeneous reactions, Atmos. Chem. Phys., 20, 6435-6453, 10.5194/acp-20-6435-2020, 2020.

Zhou, Y., Hakala, S., Yan, C., Gao, Y., Yao, X., Chu, B., Chan, T., Kangasluoma, J., Gani, S., Kontkanen, J., Paasonen, P., Liu, Y., Petaja, T., Kulmala, M., and Dada, L.: Measurement report: New particle formation characteristics at an urban and a mountain station in northern China, Atmos. Chem. Phys., 21, 17885-17906, 10.5194/acp-21-17885-2021, 2021.

Table caption

Table 1 Mass concentrations of species in the $PM_{2.5}$ samples and the meteorological conditions at the two sampling sites.

Figure captions

Figure 1 (a) Location of the study sites in China, (b) topographic view of Mt. Hua with the sampling sites marked, and (c) vertical views of the two sampling sites and the horizontal distance between them. (The maps are produced by mapbox, https://account.mapbox.com/, last access, 31 Dec. 2021).

Figure 2 Time series of the temperature (T), relative humidity (RH), boundary layer height (BLH) and mass concentrations of $PM_{2.5}$ and the water-soluble ions in $PM_{2.5}$ during the observation period at the two sampling sites.

Figure 3 Diurnal variations in $PM_{2.5}$ and the boundary layer height (BLH) at the different observation sites.

Figure 4 Concentration-weighted trajectory (CWT) analyses of $PM_{2.5}$ in both the daytime (8:00-20:00) and nighttime (21:00-7:00) at the MS site.

Figure 5 The distribution of averaged diurnal divergence over the whole campaign, with corresponding wind filed. (a) Horizontal distribution at surface. (b) Longitude-pressure cross-sections at 34°29′N. Wind speeds were represented by arrows sizes, and the W component of wind vectors was magnified 10 times.

Figure 6 Mass closure of $PM_{2.5}$ during the observed period (OM=1.6×OC).

Figure 7 Comparison of the calculated and observed NH_4^+ concentrations at the MF and MS sampling sites.

Figure 8 Schematic of the physicochemical behaviors of nitrate and ammonium during the transport process.

Figure 9 Temperature dependence of the ratio of the product of the partial pressures of NH_3 and HNO_3 with the dry dissociation constant of NH_4NO_3.

Figure 10 Nitrate and ammonium $\delta^{15}N$ values at the two sampling sites in the daytime.

Table 1 Mass concentrations of species in the $PM_{2.5}$ samples, pH and the meteorological conditions at the two sampling sites.

	Mountain foot	Mountainside
(i) Mass concentration of species and ALWC (μg/m^3) and pH		
SO_4^{2-}	10.1±6.4	9.0±7.1
NO_3^-	6.1±6.3	3.8±5.8
NH_4^+	3.9±3.3	3.9±3.5
Cl^-	0.4±0.5	0.37±0.50
Na^+	0.70±0.8	0.47±0.62
K^+	0.2±0.3	0.37±0.5
Mg^{2+}	0.1±0.1	0.07±0.06
Ca^{2+}	2.5±2.0	0.9±1.2
OC	14.0±4.7	5.0±2.8
EC	4.3±2.0	1.1±0.7
$PM_{2.5}$	76.0±44.1	47.0±38.0
ALWC	27.6±63.9	26.9±71.4
pH	3.4±2.2	2.9±2.0
(ii) Meteorological parameters		
T (°C)	23.2±4.2	15.0±2.5
RH (%)	68.9±18.2	62.8±20.0
Wind speed (m/s)	1.3±1.1	3.2±2.0
Visibility (km)	14.1±9.5	22.2±12.1

ALWC and pH are predicted by the thermodynamic model (E-AIM (IV))

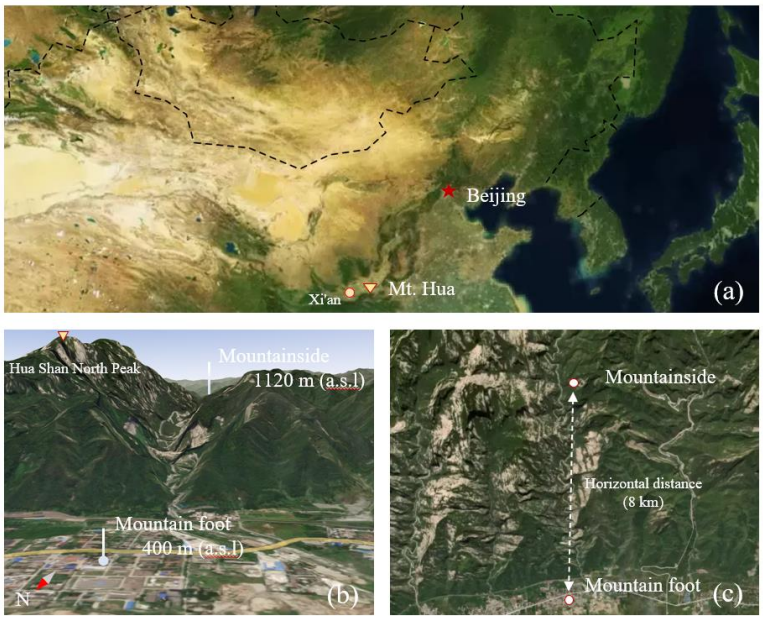

Figure 1 (a) Location of the study sites in China, (b) topographic view of Mt. Hua with the sampling sites marked, and (c) vertical views of the two sampling sites and the horizontal distance between them. (The maps are produced by mapbox, https://account.mapbox.com/, last access, 31 Dec. 2021).

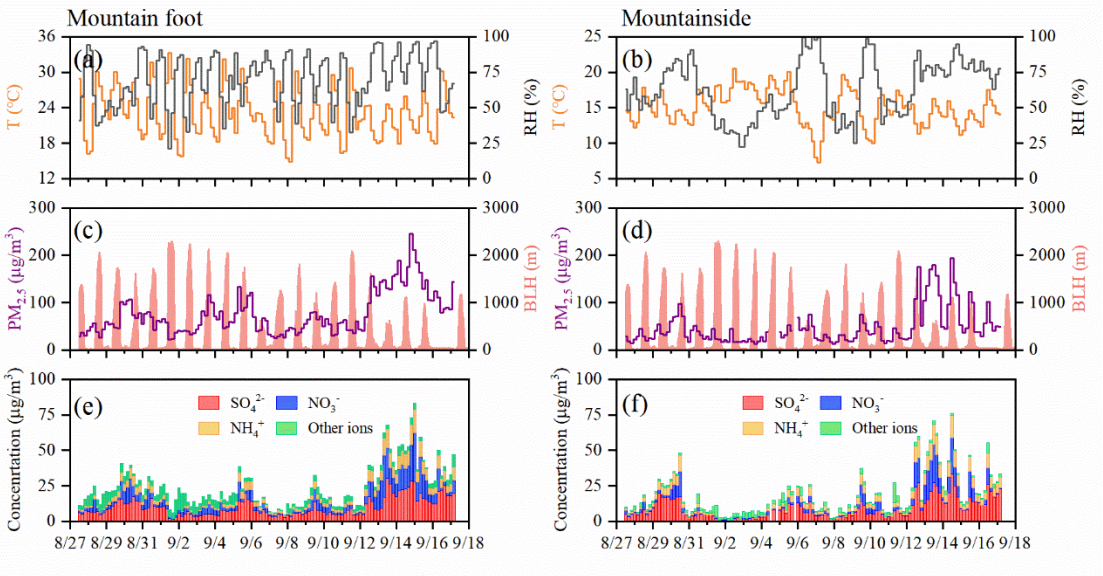

Figure 2 Time series of the temperature (T), relative humidity (RH), boundary layer height (BLH) and mass concentrations of $PM_{2.5}$ and the water-soluble ions in $PM_{2.5}$ during the observation period at the two sampling sites.

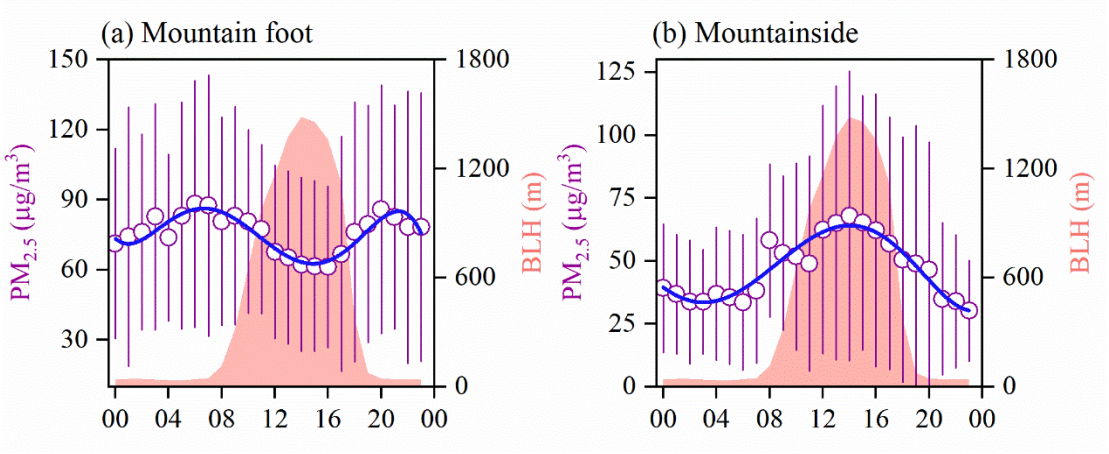

Figure 3 Diurnal variations in $PM_{2.5}$ and the boundary layer height (BLH) at the two sampling sites.

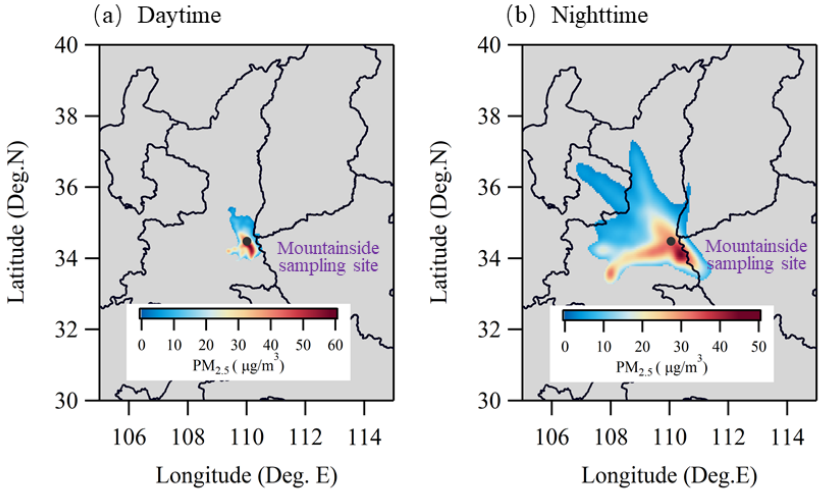

Figure 4 Concentration-weighted trajectory (CWT) analyses of $PM_{2.5}$ in both the daytime (8:00-20:00) and nighttime (21:00-7:00) at the MS site.

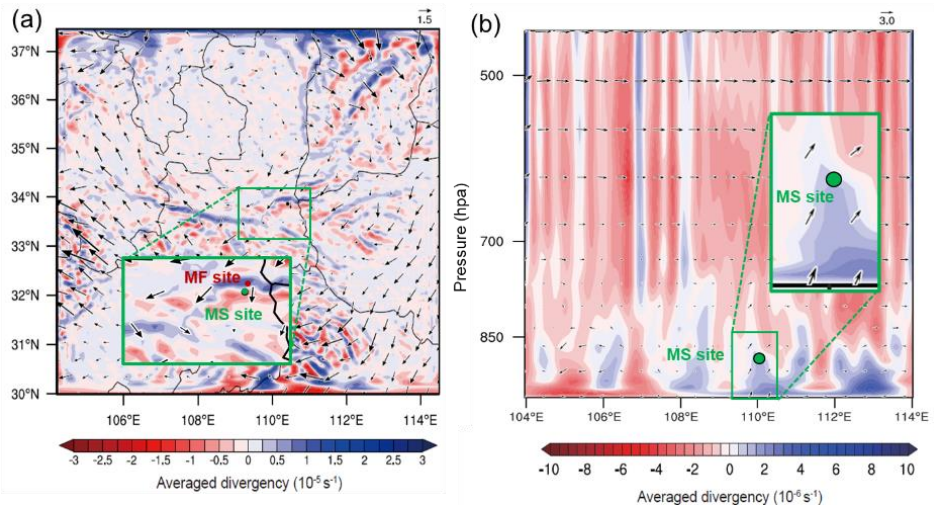

Figure 5 The distribution of averaged diurnal divergence over the whole campaign, with corresponding wind filed. (a) Horizontal distribution at surface. (b) Longitude-pressure cross-sections at 34°29′N. Wind speeds were represented by arrows sizes, and the W component of wind vectors was magnified 10 times.

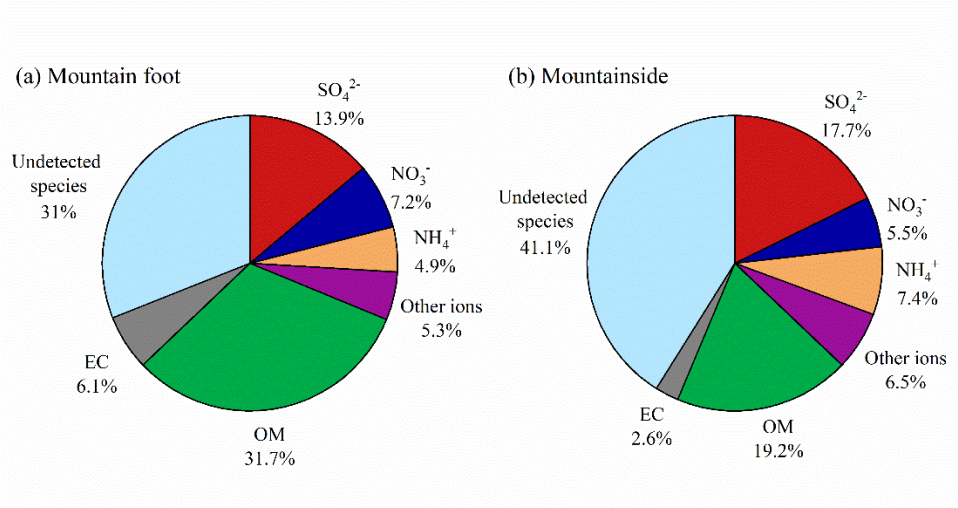

Figure 6 Mass closure of $PM_{2.5}$ during the observed period (OM=1.6×OC).

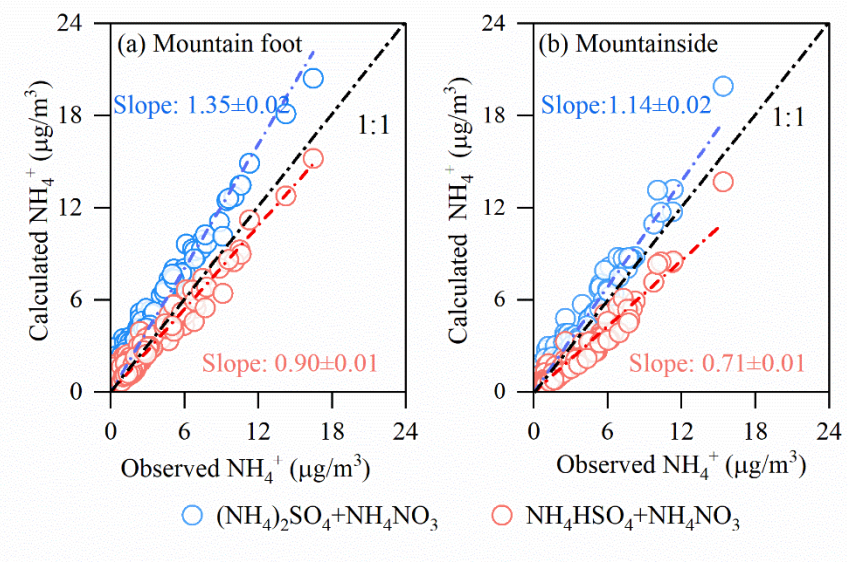

Figure 7 Comparison of the calculated and observed NH_4^+ concentrations at both sampling sites.

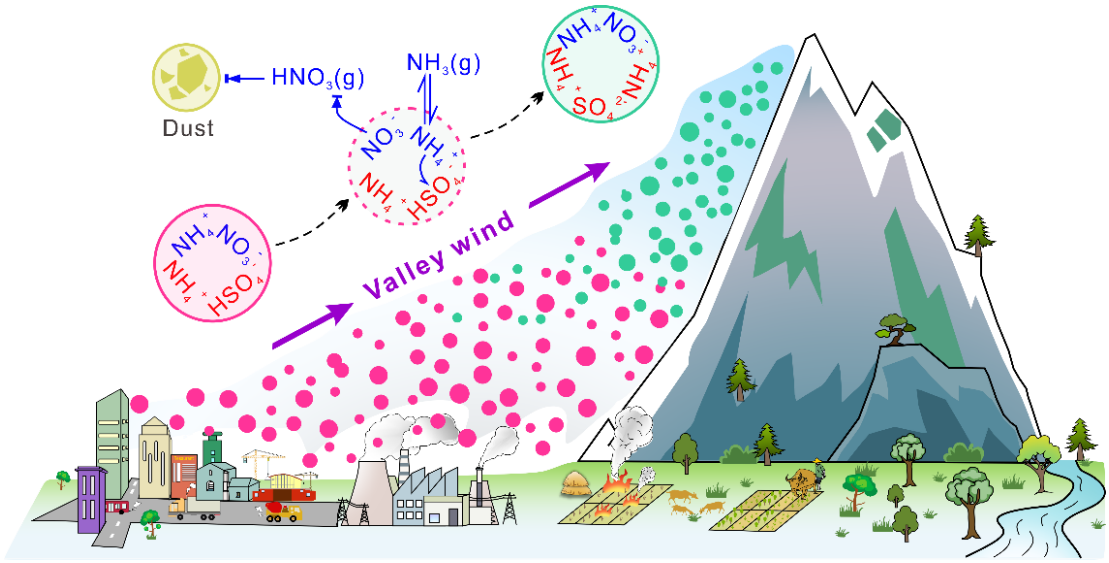

Figure 8 Schematic of the physicochemical behaviors of nitrate and ammonium during the transport process.

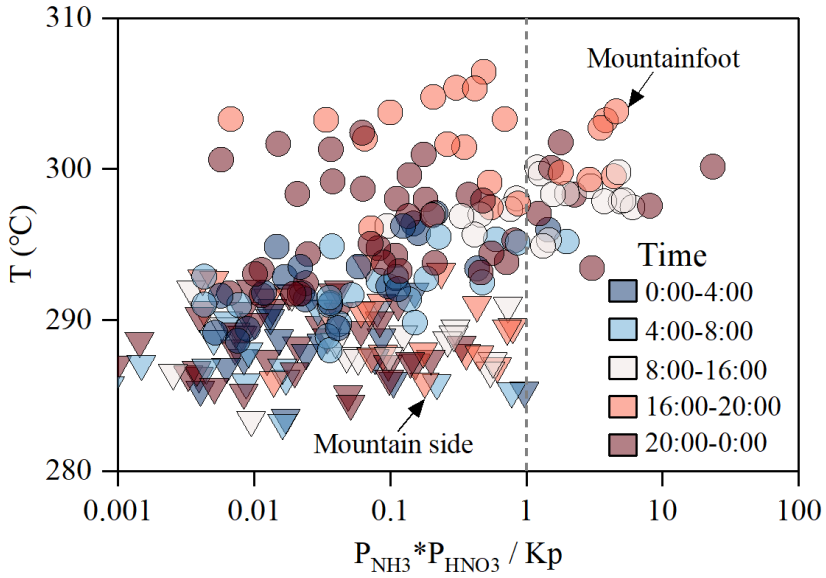

Figure 9 Temperature dependence of the ratio of the product of the partial pressures of NH_3 and HNO_3 with the dry dissociation constant of NH_4NO_3.

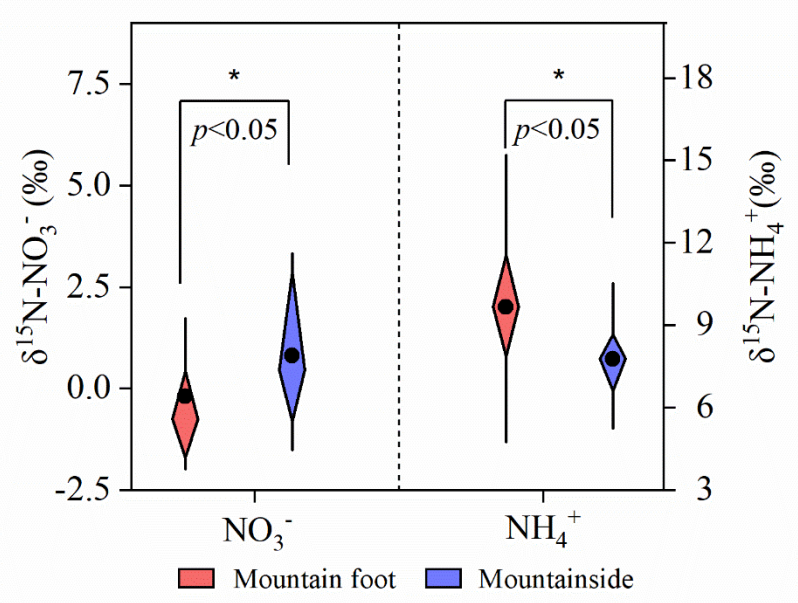

Figure 10 Nitrate and ammonium $\delta^{15}N$ values at the two sampling sites in the daytime.